Functional State of the Axonemal Dyneins during Flagellar Bend Propagation

D. M. Woolley and G. G. Vernon
Department of Physiology, School of Medical Sciences, University of Bristol, Bristol BS8 1TD, United Kingdom

ABSTRACT When mouse spermatozoa swim in media of high viscosity, additional waves of bending are superimposed on the primary traveling wave. The additional (secondary) waves are relatively small in scale and high in frequency. They originate in the proximal part of the interbend regions. The initiation of secondary bending happens only in distal parts of the flagellum. The secondary waves propagate along the interbends and then tend to die out as they encounter the next-most-distal bend of the primary wave, if that bend exceeds a certain angle. The principal bends of the primary wave, being of greater angle than the reverse bends, strongly resist invasion by the secondary waves; when a principal bend of the primary wave propagates off the flagellar tip, the secondary wave behind it suddenly increases in amplitude. We claim that the functional state of the dynein motors in relation to the primary wave can be deduced from their availability for recruitment into secondary wave activity. Therefore, only the dyneins in bends are committed functionally to the maintenance and propagation of the flagellar wave; dyneins in interbend regions are not functionally committed in this way. We equate functional commitment with tension-generating activity, although we argue that the regions of dynein thus engaged nevertheless permit sliding displacements between the doublets.

INTRODUCTION

The mechanisms underlying flagellar coordination are difficult to investigate and still largely unknown. Any newly discovered pattern of movement may be a source of clues to these mechanisms. We have noticed that when mammalian spermatozoa swim in viscous media, two types of traveling wave may coexist in the same plane on the flagellum. There is the familiar large-scale waveform that originates at the neck; and there is a superimposed, smaller-scale waveform that occurs only distally. We found it initially puzzling how the dyneins at any given location in the axoneme could avoid being "confused" over which waveform they were actively generating. A resolution of the puzzle has emerged from our analysis, namely, that when the primary wave travels along the flagellum, it is only in certain parts of the wave that the dyneins are functionally committed to its maintenance. This is deduced from the uninvolvement of those parts in secondary wave activity. Close inspection of the secondary waves is thus an indirect way of probing the function of axonemal dyneins in bend propagation.

Our analysis of the two types of wave began with repeated slow-motion replay of videotape recordings. But it became important to know the patterns of sliding displacement taking place during bend growth and propagation. The remainder of this Introduction will be a brief explanation of the long-established method for studying these displacements.

The method, shear curve analysis, is based upon several assumptions. For a planar waveform, it is assumed that no sliding is possible at the base, that there is no torsion about the local axis, that the doublet microtubules are neither extensible nor compressible, and that the axonemal cylinder retains its circular cross-sectional profile and has a constant diameter. With these provisions, the amount of sliding at any given position (s) along the flagellum is proportional to the shear angle at position s. The shear angle is the angle of intersection between the tangent to the waveform at position s and the tangent to the waveform at the base of the flagellum. A shear curve describes the relative amounts of sliding at all positions on the flagellum at a given instant; a family of shear curves shows how these sliding displacements change with the phase of the beat cycle. Shear curves resemble waveforms but in a potentially confusing way, because the bends on the wavelike shear curve correspond to the regions between the bends on the flagellum; conversely, the regions between the bends on the shear curve correspond to the bends on the flagellar wave. The analysis of such curves has been given a formal exposition by Gibbons (1981b, 1982) and, in summary form, by Brokaw (1991).

The study of shear curves has resulted in the recognition of several patterns of sliding (Gibbons, 1981b, 1982). We shall present these patterns for mouse spermatozoa and show that the superimposition of waves illustrates a long-standing problem in the application of the sliding doublet theory to planar flagellar waves: namely, how is it possible for sliding displacements to occur throughout existing bends without disturbing them? Can a new bend grow at the proximal end without causing sliding to occur throughout the established bends that are propagating on the distal flagellum? It cannot unless the new bend grows to half its final angle at the same time as the preceding bend completes the second half of its growth, with the final magnitude of the first pair of bends being equal (Goldstein, 1975, 1976,

Submitted April 15, 2002, and accepted for publication May 29, 2002.

Address reprint requests to Dr. David M. Woolley, Department of Physiology, School of Medical Sciences, University of Bristol, Bristol BS8 1TD, UK. E-mail: d.m.woolley@bristol.ac.uk.

0006-3495/02/10/2162/08 $2.00

1977). Otherwise, as is commonly the case, the development of new bends does require sliding throughout established, propagating bends; it is described as synchronous sliding (Gibbons, 1981b). Synchronous sliding, then, presents a major conceptual difficulty: if one accepts that resistances to sliding must be operating in the transformation of sliding into bending (reviewed by Gibbons, 1981a), then how can a given region of axoneme both resist and permit sliding simultaneously? Not surprisingly, the reality of synchronous sliding has been closely questioned. Our study, however, has convinced us of the reality of synchronous sliding, through the recognition that sliding related to primary wave propagation must in some situations pass through the bent regions of secondary waves, constituting a new class of synchronous displacement.

MATERIALS AND METHODS

Adult male mice (CD1 strain) were killed by cervical dislocation. After 30 min, spermatozoa were removed from each cauda epididymidis and suspended in Hanks' balanced salt solution containing 3 mg/ml bovine serum albumin (fraction V, Sigma Chemical Co., St. Louis, MO) at room temperature. A slide chamber ~80 μm deep (i.e., a supported coverslip) was prepared containing a droplet (25 μl) of Hanks' balanced salt solution containing bovine serum albumin and 2% methyl cellulose (Sigma, catalog items M0387 and M0512) so as to raise the viscosity to, nominally, 400, 1500, or 4000 cP (0.4, 1.5, or 4.0 Pa s). In some trials, calcium was omitted from the Hanks' solution, and 250 μM EGTA was added. The sperm suspension was then run into the chamber so as to form an interface with this droplet. The observations were made at room temperature (22–24°C). We report here on the motility of spermatozoa that swam into the viscous medium and moved in a planar fashion just beneath the coverslip. The Leitz Ortholux II microscope was fitted with a 100-W quartz-iodide lamp, a heat filter, and an UV barrier filter. Illumination was through an oil-immersion dark-field condenser. Observations of flagellar bending were made using a ×40 planachromat oil objective. The motility was recorded on sVHS videotape using a 50-Hz (CCD) camera and a Panasonic (AG7350) VCR linked to a video timer (model VTG33F, For.A, Tokyo, Japan).

To plot the shear curves, suitable movies of individual sperm were captured on a PC using Scion Image software (Scion Corp., Frederick, MD) and a Scion LG-3 scientific frame grabber. Raw movies were then suitably processed and transferred to a PowerMac. Individual frames were then analyzed using a version of NIH Image modified to allow curve tracing of flagellar images (available at http://www.cco.caltech.edu/~brokawc/software.html) (Brokaw, 1990). Each flagellar image was curve fitted with 120 1-μm straight segments. Multiple curves were fitted to each flagellar image; these data sets were then averaged to remove noise. The data are plotted normalized to a point 3 μm distal to the base of the flagellum. This point represents the first free point of the flagellum, i.e., where it is not in close contact with the sperm head/neck apparatus.

The curve-fitting program had been designed for use with images of sea urchin spermatozoa. Because we were applying it to mammalian spermatozoa, it was necessary to adjust the shear angles to take account of the taper of the axonemal complex. We assume that the doublet-outer dense fiber complex slides as a single structure. Therefore the effective diameter (the constant of proportionality to express shear angle as linear displacement) is greater than the axonemal diameter where the outer dense fibers are present, i.e., in the proximal flagellum. We have taken the maximum effective diameter to be 0.28 μm (Fig. 1) and, as an approximation, considered it to reduce at a constant rate to 0.20 μm proximo-distally. The adjusted shear angle is thus made proportional to the sliding displacement.

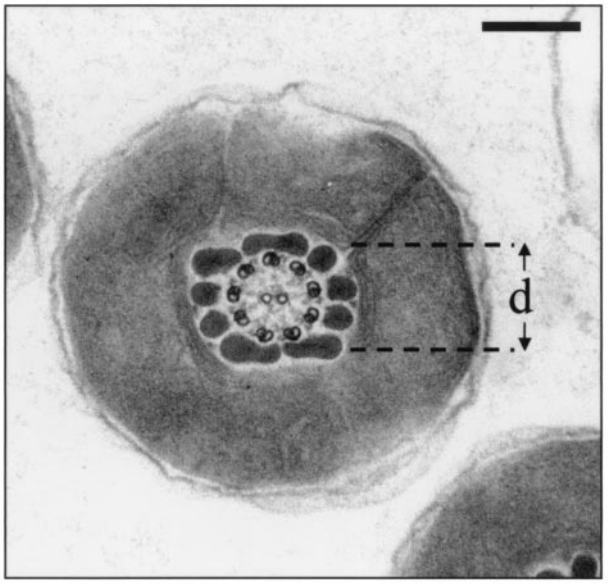

FIGURE 1 An electron micrograph of a thin transverse section of the sperm flagellar midpiece of the mouse. The nine outer dense fibers lie between the 9 + 2 axoneme and the mitochondrial sheath. For the purpose of adjusting the shear angles, the distance d is taken as the maximal effective diameter of the tapering axonemal complex. Scale bar, 0.2 μm.

Transmission electron micrographs were prepared by a standard method (Woolley, 1977).

RESULTS

We have seen the phenomenon of wave superimposition in the spermatozoa of the rat, bull, chinchilla, golden hamster, and mouse. Mouse sperm were chosen for detailed analysis because it was helpful to have both head and bend asymmetries, strict planarity, and as many as two cycles of bending on the flagellum. The large-scale waveform originating at the neck will be called the primary wave. The smaller-scale waveform on the distal flagellum will be called the secondary wave. The combination of a primary wave with secondary waves will be known as a complex wave. The phenomenon of complex waves was not dependent on the presence of calcium ions in the medium.

The primary and secondary waves are different in how they originate. Bend growth in the primary wave occurs mainly in the most proximal bend; growth and propagation tend to be distinct and sequential. The secondary waves, however, begin as low-amplitude vibratory activity and grow markedly in amplitude during their propagation. By this criterion, it is possible to say that secondary waves can exist on the distal flagellum in the absence of a primary wave. This is seen in pathological states, for example, where the flagellum has a fixed curvature or a loop in the proximal part (not illustrated).

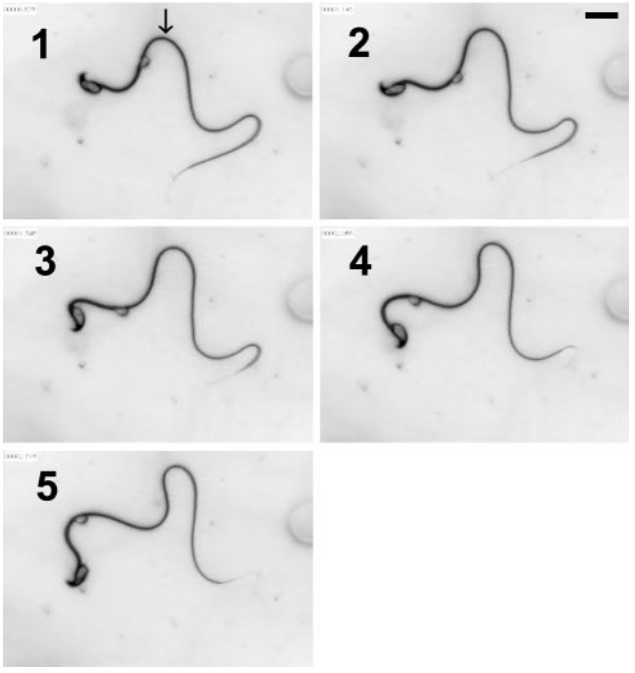

FIGURE 2 A sequence of dark-field video micrographs (contrast reversed) to show one cycle of the primary wave. These are the images used in the construction of the shear curves of Fig. 3. When a bend is in the direction arrowed, it is defined as a principal (P) bend. Scale bar, 5 μm.

Sperm flagella with only a primary wave

This type was unusual in these conditions but makes a useful starting point because the geometrical simplicity will serve to introduce the terminology and explain the standard way in which the shear curves are interpreted.

From the micrograph set (Fig. 2), it can be seen that the waveform is planar. The asymmetrical (falciform) structure of the sperm head means that the bends on opposite sides of the flagellum can always be distinguished. By convention (Woolley, 1977), a bend in the direction of that arrowed in Fig. 2 is a principal (P) bend; a bend in the opposite direction is a reverse (R) bend. The P bends consistently develop greater angles than R bends in these conditions. This bend asymmetry causes the sperm to swim in circular paths.

Fig. 3 shows the set of shear curves derived from the images in Fig. 2. It represents one typical cycle of bending. Each of the five curves is the plot of the local shear angle for 120 successive positions along the flagellum. The presentation of these curves follows closely the style established by Gibbons (1981b, 1982) whose papers contain a more formal and extended explanation.

Regions of a curve that have a positive gradient correspond to P bends; regions with negative gradient represent R bends. Inflection regions at the top of each shear curve represent interbend regions between P and R bends; inflection regions at the bottom correspond to R-P interbend regions of the flagellum. The proximal flagellum shows increases in the amplitude of the curve that represent the development of the bends. The curvature of a bend (radians per micron) is given by the slope. An increase in curvature during propagation was seen for P bends but not for R bends. As indicated in the Introduction, the types of sliding

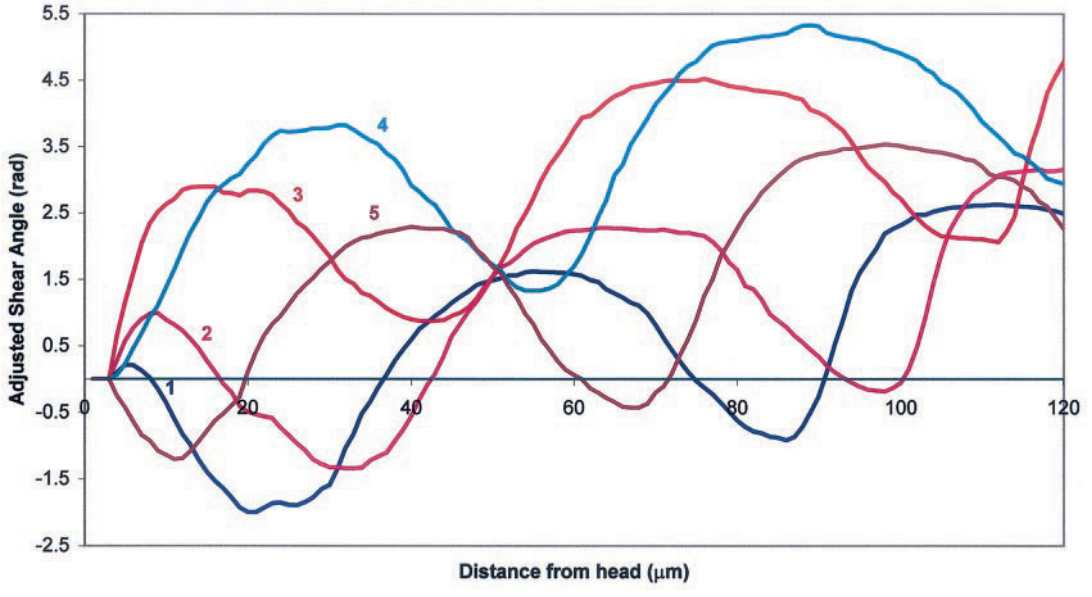

FIGURE 3 The family of six shear curves numbered to show the correspondence with the six video frames of Fig. 2. The adjustment made to the shear angles was to allow for the taper of the axonemal complex. Each curve is the average of five repetitions of the curve-fitting process. This family of curves is used to explain how shear curves are interpreted (see text). The time interval between successive curves is 466 ms.

that occur during bend formation and bend propagation are revealed by the set of curves. (1) Metachronal sliding is the sliding displacement associated with the propagation of a bend over any point on the distal flagellum. (2) Nonoscillatory synchronous sliding is a necessary correlate of bend asymmetry and is detected from the shear curve envelope when the time-averaged value of the shear angle at the tip of the flagellum has a positive value. This was a characteristic feature in the mouse spermatozoa analyzed here. (3) Oscillatory synchronous sliding results when the most proximal bend (whether P or R) begins its development after the previously formed bend has developed fully or at least has grown to more than half its final angle. The motility pattern in this case is notable for pronounced yaw of the head. The diagnostic feature in the set of shear curves is the constriction of the envelope. Constriction down to a point, as is almost the case in Fig. 3 at ~46 and 110 μm along the flagellum, indicates that bend development is almost wholly a result of oscillatory synchronous sliding. This was typical for the mouse spermatozoa swimming in viscous media.

Sperm flagella with superimposed waves

Secondary waves were superimposed on the primary wave in almost all the spermatozoa when the viscosity of the medium was 0.4–4.0 Pa s.

The geometrical relationship of secondary waves to the primary waveform will be described qualitatively. Secondary waves were seen only on the distal half of the flagellum. They took their origin as symmetrical wavelets only in the interbends of the primary wave, specifically in the most proximal part of the interbend. Those that propagated along an R-P interbend did not invade the preceding P bend, whereas those running on a P-R interbend typically did invade the preceding R bend and ran around its curvature, the secondary wave thereby becoming asymmetrical. The inhibitory action of the P bends on the amplitude and propagation of secondary waves proximal to them was clear: as each P bend was lost from the tip, there was heightened bend development in the following secondary wave. These features are illustrated by a single typical cycle of the primary wave, shown as a set of micrographs (Fig. 4) and also as a set of six derived shear curves (Fig. 5). To show the consistency of these findings, sets of shear curves from two other spermatozoa are included (Fig. 6). When Figs. 5 and 6 are compared with Fig. 3 the oscillations in shear angle associated with the secondary waves are confirmed as being found distally, most prominently on the P-R interbend, also on the R bend, and less prominently on the R-P interbend until the P bend runs off the tip. As already mentioned the secondary wave began as a very 1ow-amplitude motion (Fig. 7).

When one examines the envelope of the primary wave in each of Figs. 5 and 6, it shows the same characteristics as that in Fig. 3, namely (1) an upward slope of the mean shear angle from base to tip, indicating nonoscillatory synchronous sliding, and (2) a marked constriction at a point 50–60 μm along the flagellum, indicating that new bend growth is largely achieved by oscillatory synchronous sliding. The point of constriction of the envelope represents a place on the axoneme that experiences little or no interdoublet sliding.

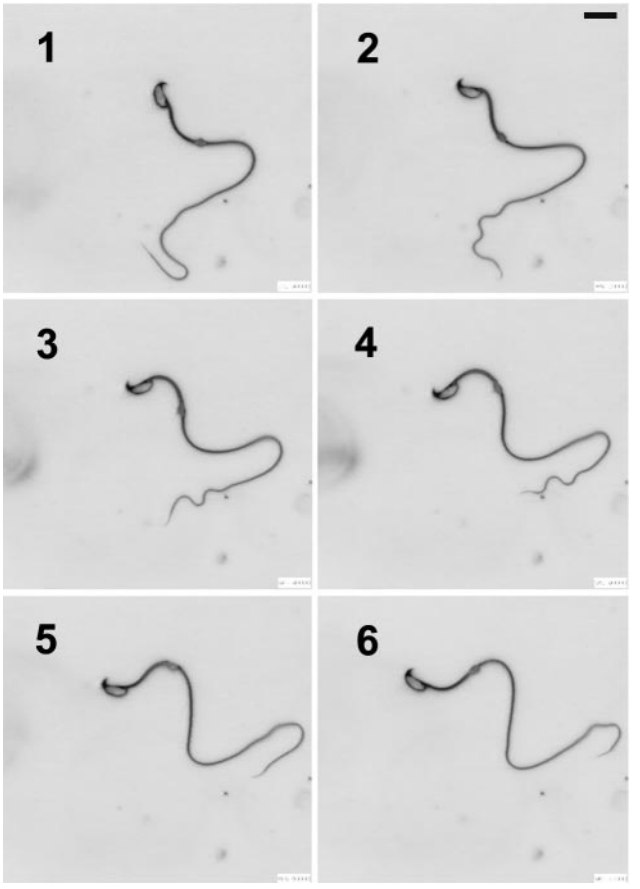

FIGURE 4 Another sequence of micrographs showing now a sperm with a complex wave (secondary waves upon the primary wave). Scale bar, 5 μm

We estimated the beat frequencies of the two types of wave for a large sample of spermatozoa at viscosity 1.5 Pa s. The beat frequency of the secondary wave, f_2 (range, 2.3–5.9 Hz) was on average 15 times greater than that for the primary waves, f_1 (range, 0.178–0.42 Hz). We looked for but could not establish a significant correlation between the two frequencies ($r = 0.31$; $n = 24$). For the sperm shown in Figs. 4 and 5 the estimates of f_1 and f_2 were 0.22 and 4.31 Hz, respectively. The velocity of propagation of the primary wave (v_1) was measured from Fig. 5 to be 12 μm s^{-1}, similar to the value of 14.7 μm s^{-1} calculated from frequency and wavelength ($f_1 \times \lambda_1$). The measured velocity of the secondary wave (v_2) was 52 μm s^{-1} (obtained from Fig. 7, a more frequent sampling of the Fig. 5 set of shear curve). Calculating v_2 from ($f_2 \times \lambda_2$) gives a value of only

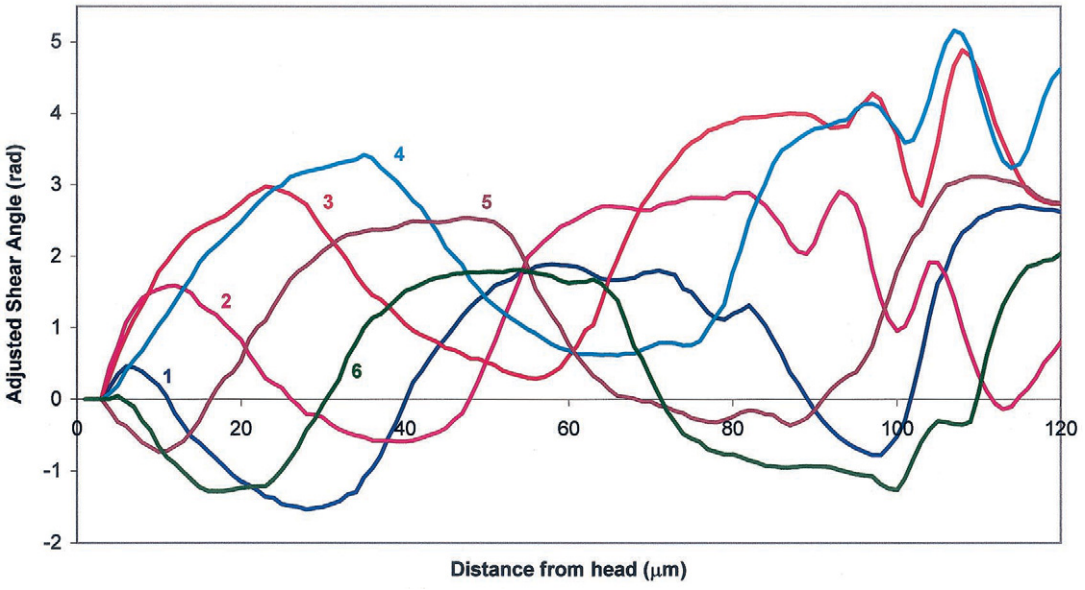

FIGURE 5 The family of six shear curves derived from the video frames of the complex wave in Fig. 4. The interval between successive curves is 700 ms (for interpretation, see text).

37 μm s^{-1}. It thus appears that $v_{2,\text{actual}} = (v_{2,\text{calculated}} + v_1)$, a result consistent with the moving origin of the secondary wave.

What has been described in this section is a general pattern. Some exceptional events have been observed, namely, invasion of P bends near the tip of the flagellum by secondary waves and noninvasion of R bends when their angle was greater than the typical magnitude. We have also seen P bends become smaller and smaller toward the tip until they propagate as components of the secondary waves behind them.

DISCUSSION

Superimposed traveling waves can exist on mammalian sperm flagella when the viscosity of the medium is high. Mammalian spermatozoa do swim in viscous media after they have entered the female tract. Possibly, then, the secondary waves have a physiological role in optimizing propulsion. But we cannot relate complex waves to hyperactivation behavior (Suarez and Dai, 1992) because they occur in the absence of calcium in the external medium. Our study has focused on the implication of complex waves for the general mechanism of the axoneme. How can two different waves travel in the same plane on a single axoneme? (Although superimposed waves have been reported before (Vernon and Woolley, 1999), the primary waves in such cases have been helical and could have been established passively.) We have considered two classes of explanation.

First, there may be two motor systems within the flagellum. The mammalian sperm flagellum contains nine outer dense fibers in its proximal part (seen in Fig. 1). Could these nine fibers generate the primary waveform, with the simple axoneme generating the secondary waves? The primary wave would dominate activity proximally, as one observes. Secondary wave activity might originate at the flagellar base but remain latent until it reached the distal axoneme. However, there is a consensus view that these outer dense fibers are passive structures (see references in Kim at al., 1999). As stiff, passive structures, they may well have an influence on the complex wave by inhibiting the development of secondary waves on the proximal part of the flagellum, where they are thickest. The possibility that outer dense fibers are essential for generating the complex waves could be ruled out by discovering complex waves on a simple 9 + 2 flagellum.

Another speculative explanation could be that the two motor systems are, in fact, the outer and inner sets of dynein arms. Brokaw (1996) has modeled responses to viscous load in terms of differential inner/outer arm function. Although his findings could have other explanations (such as drag experienced by the sperm head), it is an attractive possibility that the primary and secondary waves are generated by different classes of dynein. There is as yet no evidence to support it, but the idea is testable in principle.

Second, there may be a single motor but with only parts of it engaged in the primary wave, leaving other parts available for secondary activity. Our preferred interpretation is that the axonemal dyneins change between two functional states during primary wave travel. In one state they are committed to maintaining the primary wave; for the rest of the time they are uncommitted. Uncommitted dyneins are available to be recruited into a commitment to secondary waves. One can thus identify the regions of

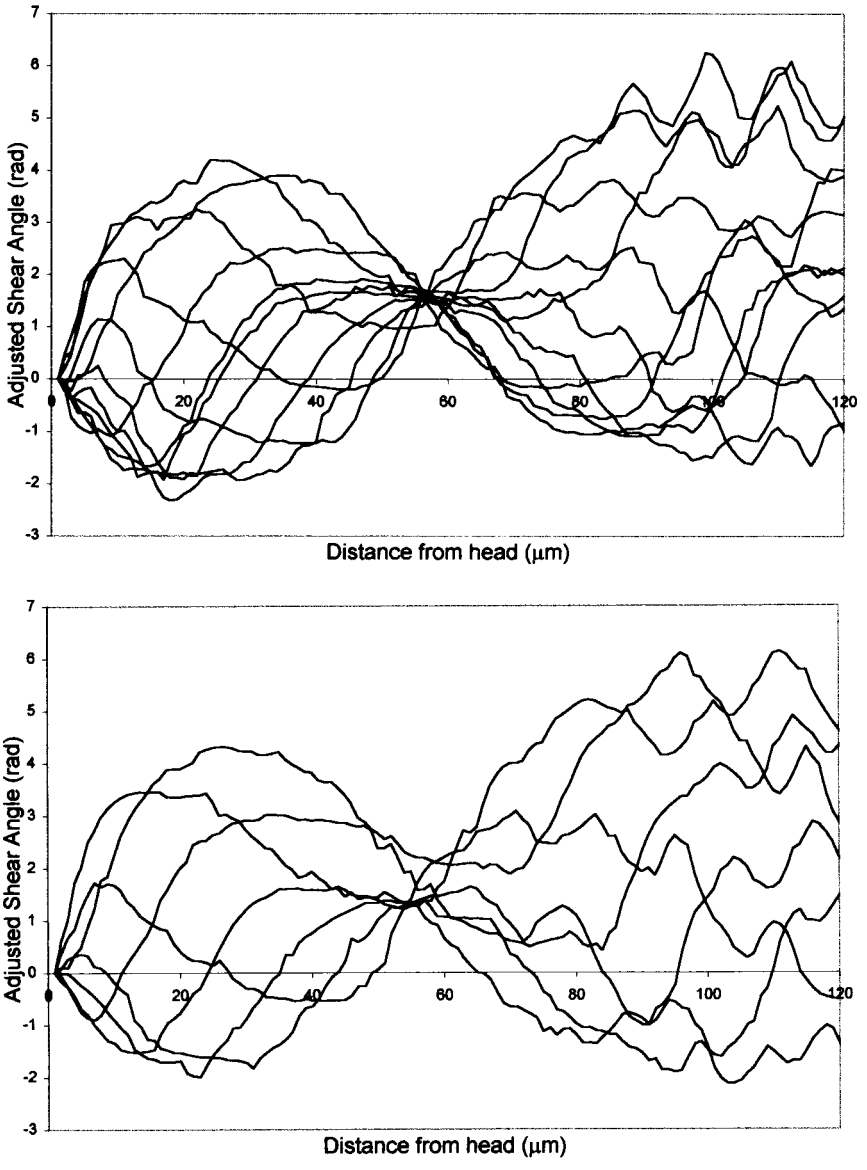

FIGURE 6 Two additional examples of sets of shear curves derived from video sequences (not shown) of complex waves. In these examples, no averaging has been performed.

dynein arms that are committed to the primary wave by identifying the regions of the primary wave that are not expressing secondary wave activity.

The idea of a traveling zone of commitment is consonant with our earlier experimental work (Vernon and Woolley, 1995). Using long ribbons of doublets and exposing them uniformly to ATP (through caged ATP photolysis), we found that the mechanical response, tension development, was localized and propagated from base to tip. Zonal activation of tension development obviously meant that on either side of the zone, the dyneins were inactive, even though they were exposed to physiological levels of ATP.

At this point we draw the conclusion that for the distal flagellum of the mouse spermatozoon the zones of commitment correspond to the P bends of the primary wave. Why not also the R bends? At present, we suggest that the explanation lies in the extreme beat asymmetry of the specimens studied. We suggest that the zone of commitment underlying the smaller-angle R bends is less developed from the outset and decays completely on the distal flagellum. As we have mentioned (Results), we have occasionally seen waves that were more symmetrical and had R bends of large angle that (like the P bends) were devoid of secondary waves. We have seen this repeatedly in an unpublished study of rat spermatozoa. We have also occasionally seen, in mouse sperm, P bends invaded by secondary waves when they reached an extreme distal position. Thus we do not propose a fundamental distinction between the P and R bends of the primary wave. The distinction drawn is between bends and interbends, consistent with the recognition of the waveform as a succession of arcs and lines (Brokaw, 1965). It is relevant that, in simpler 9 + 2 flagella, the bends

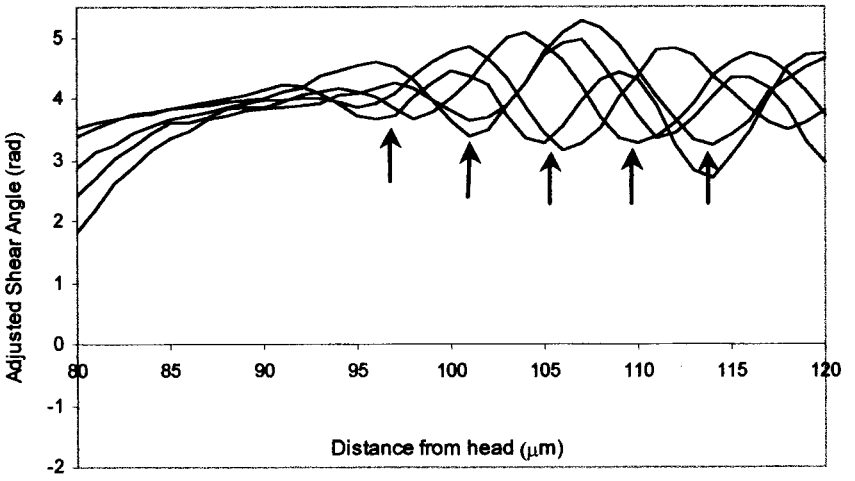

FIGURE 7 Part of the shear curve set shown as Fig. 5, prepared in the same way but expanded to provide greater time resolution and allow individual secondary bends to be followed. Only the distal flagellum is shown. The interval between curves is now 100 ms. The arrows indicate the propagation of an R-P interbend region.

are the inflexible regions whereas the interbends are prone to sliding adjustments and torsions during propagation (see Woolley and Vernon, 2001). In the above, we are equating pronounced functional commitment with a bend of large angle. We have to accept, however, that high curvature, imposed by propagation into a high-viscosity medium, might per se suppress the recruitability of dyneins into secondary wave activity. Curvature inhibition has been considered as a regulatory principle in flagellar oscillation (Brokaw 1980, 1982).

We have implied that the state of dyneins in the large-angle bends of the primary wave is equivalent to a state of active tension development. Should such a state be equated with a resistance to inter-doublet sliding? Are secondary waves impossible here just because there is resistance to sliding? It is commonly stated that serially operated resistances to sliding on the distal flagellum are necessary, and several candidate structures have been proposed (reviewed by Gibbons 1981a, Woolley and Bozkurt, 1995). Whether or not sliding is occurring can be discovered only by shear curve analysis. In the following paragraph, the question of sliding in the P bends of the primary wave will be looked at critically. In summary, we shall conclude that inter-doublet sliding does occur in these sites.

Should sliding throughout the established bends of the primary wave be believed? The phenomenon is called synchronous sliding (see Introduction) and is a purely geometrical idea implying nothing about the behavior of the dynein arms (Gibbons, 1981b, 1982). The envelopes of the shear curves in Figs. 3, 5, and 6 provide indisputable evidence of both oscillatory and nonoscillatory synchronous sliding (Gibbons, 1981b, 1982), if the assumptions of the method are true. Now, the important assumptions can be seriously questioned. First, the resting state of the flagellum might well be curved, which would make it unnecessary to accept nonoscillatory synchronous sliding. Second, there is recent evidence that basal sliding does occur in mammalian sperm flagella; it is accommodated by compression of the connecting piece (Vernon and Woolley, 2002). This could make it unnecessary to accept oscillatory synchronous sliding. (However, this consideration is unlikely to apply to simpler (9 + 2) axonemes for which there is experimental evidence of oscillatory synchronous sliding (Brokaw, 1991).) Despite these reservations, there seems to us to be a new demonstration of synchronous sliding in the results we present here. Consider the propagation of a secondary wave around the curvature of a traveling R bend, and consider the bends of that secondary wave. The shear curves tell us that metachronal sliding associated with the propagation of the R wave must be running through the bends of the secondary wave. We identify this as an extra class of synchronous sliding, meta-synchronous sliding. Because of this we continue to believe that bends propagating along the axoneme must be regions where inter-doublet sliding is possible.

Having argued for the reality of synchronous sliding, we admit that we do not know how this is compatible with sustaining tension on the axoneme as a whole, but it could be, perhaps, that the short duty ratio of the outer dynein arms (Howard, 2001) permits both activities simultaneously. If sliding in the primary bends is accepted, then the inability of the secondary wave to invade them cannot be attributed to a restriction on sliding. We propose instead that it is due to a nonrecruitable state of the dynein, that the pattern of activation here is already determined. For this reason, also, the primary bends cannot function as the sites of origin of the secondary wave. One current idea regarding the origin of planar flagellar oscillations is that a regular and sustained oscillation can only be established distal to a site of doublet anchorage, normally the transition zone/basal body assembly (see Woolley and Bozkurt, 1995, and references therein). Our observations apparently mean that the oscillation can also originate in uncommitted dyneins distal to a zone of (presumed) active tension development.

We thank Dr. Charles Brokaw for making available his computer program for automatic curve fitting and for his advice on its application. Thanks also to Debbie Carter for editing the videotape sequences and producing the shear curves.

Our work on flagellar mechanisms is currently supported by the Biotechnology and Biological Sciences Research Council (U.K.) grant 7/C11957.

REFERENCES

Brokaw, C. J. 1965. Non-sinusoidal bending waves of sperm flagella. *J. Exp. Biol.* 43:155–169.

Brokaw, C. J. 1980. Theoretical models for oscillation and bend propagation by sperm flagella. *In* Testicular Development, Structure and Function. A. Steinberger and E. Steinberger, editors. Raven Press, New York. 447–453.

Brokaw, C. J. 1982. Models for oscillation and bend propagation by flagella. *Symp. Soc. Exp. Biol.* 35:313–338.

Brokaw, C. J. 1990. Computerized analysis of flagellar motility by digitization and fitting of film images with straight segments of equal length. *Cell Motil. Cytoskel.* 17:309–316.

Brokaw, C. J. 1991. Microtubule sliding in swimming sperm flagella: direct and indirect measurements on sea urchin and tunicate spermatozoa. *J. Cell Biol.* 114:1201–1215.

Brokaw, C. J. 1996. Microtubule sliding, bend initiation, and bend propagation parameters of *Ciona* sperm flagella altered by viscous load. *Cell Motil. Cytoskel.* 33:6–21.

Gibbons, I. R. 1981a. Cilia and flagella of eukaryotes. *J. Cell Biol.* 91:107s–124s.

Gibbons, I. R. 1981b. Transient flagellar waveforms during intermittent swimming in sea urchin sperm. II. Analysis of tubule sliding. *J. Muscle Res. Cell Motil.* 2:83–130.

Gibbons, I. R. 1982. Sliding and bending in sea urchin sperm flagella. *Symp. Soc. Exp. Biol.* 35:225–287.

Goldstein, S. F. 1975. Morphology of developing bends in sperm flagella. *In* Swimming and Flying in Nature, Vol 1. T.Y.-T. Wu, C. J. Brokaw, and C. Brennen, editors. Plenum Press, New York. 127–131.

Goldstein, S. F. 1976. Form of developing bends in reactivated sperm flagella. *J. Exp. Biol.* 64:173–184.

Goldstein, S. F. 1977. Asymmetric waveforms in echinoderm sperm flagella. *J. Exp. Biol.* 71:157–170.

Howard, J. 2001. Mechanics of Motor Proteins and the Cytoskeleton. Sinauer Associates, Sunderland, MA.

Kim, Y. H., J. R. McFarlane, M. K. O'Bryan, G. Almahbobi, P. D. Temple-Smith, and D. M. de Kretser. 1999. Isolation characterization of rat sperm tail outer dense fibres and comparison with rabbit and human spermatozoa using a polyclonal antiserum. *J. Reprod. Fertil.* 116: 345–353.

Suarez, S. S., and X. Dai. 1992. Hyperactivation enhances mouse sperm capacity for penetrating viscoelastic media. *Biol. Reprod.* 46:686–691.

Vernon, G. G., and D. M. Woolley. 1995. The propagation of a zone of activation along groups of flagellar doublet microtubules. *Exp. Cell Res.* 220:482–494.

Vernon, G. G., and D. M. Woolley. 1999. Three-dimensional motion of avian spermatozoa. *Cell Motil. Cytoskel.* 42:149–161.

Vernon, G. G., and D. M. Woolley. 2002. Microtubule displacements at the tips of living flagella. *Cell Motil. Cytoskel.* 52:151–160.

Woolley, D. M. 1977. Evidence for 'twisted plane' undulations in golden hamster sperm tails. *J. Cell Biol.* 75:851–865.

Woolley, D. M., and H. H. Bozkurt. 1995. The distal sperm flagellum: its potential for motility after separation from the basal structures. *J. Exp. Biol.* 198:1469–1481.

Woolley, D. M., and G. G. Vernon. 2001. A study of helical and planar waves in sea urchin sperm flagella, with a theory of how they are generated. *J. Exp. Biol.* 204:1333–1345.